

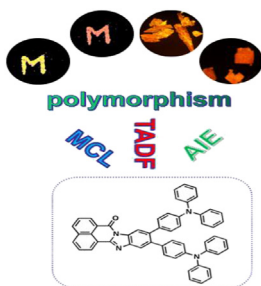


Research article

A simple molecular design towards the conversion of a MCL backbone to a multifunctional emitter exhibiting polymorphism, AIE, TADF and MCL

Bin Huang ^{a,b,1,*}, Wenbing Yu ^{a,c,1}, Li Yang ^a, Yan Li ^a, Ning Gu ^{a,**}^a State Key Laboratory of Bioelectronics, Jiangsu Key Laboratory for Biomaterials and Devices, School of Biological Science and Medical Engineering, Southeast University, Nanjing 210096, PR China^b College of Life Sciences and Chemistry, Jiangsu Key Laboratory of Biofunctional Molecule, Institute of New Materials for Vehicles, Jiangsu Second Normal University, Nanjing 210013, PR China^c Nanjing Youhealing Medical Nutrition Technology Co. Ltd, Nanjing, 211505, PR China

GRAPHICAL ABSTRACT



This work demonstrated a simple molecular design strategy towards the conversion of a MCL backbone to a multifunctional emitter exhibiting polymorphism, AIE, TADF and MCL.

ARTICLE INFO

Keywords:

Polymorphism
MCL
AIE
TADF
Triphenylamine
Benzo[*d,e*]benzo[4,5]imidazo[2,1-*a*]isoquinolin-7-one

ABSTRACT

Compared with the large number of single-function materials such as aggregation-induced emission (AIE), mechanochromic luminescence (MCL), or thermally activated delayed fluorescence (TADF) emitters, multifunctional emitting materials offer more opportunities in practical applications. In this report, we provide a simple molecular design strategy towards the conversion of a MCL building block to a multifunctional emitter. Through altering the substituent sites and increasing the number of electron donors and steric hindrance on a normal MCL backbone benzo[*d,e*]benzo[4,5]imidazo[2,1-*a*]isoquinolin-7-one, a novel multifunctional material 10,11-bis-(4-diphenylamino-phenyl)-benzo[*d,e*]benzo[4,5]imidazo[2,1-*a*]isoquinolin-7-one (10,11-2TPA-BBI) is designed and synthesized. 10,11-2TPA-BBI exhibits simultaneous polymorphism, AIE, MCL and TADF properties. It can form four different aggregate species: yellow solid (YS) and orange solid (OS), orange flake-shaped crystal (OC), and red prism-like crystal (RC). Among them, because of the small energy gaps ($\Delta E_{STs} < 0.3$ eV) between the singlet and triplet excited states, OS, OC and RC exhibit TADF properties, while YS show normal fluorescence characteristics with a large ΔE_{ST} of 0.33 eV. OS can be reversibly transformed into YS upon external stimuli, which can be attributed to the emission switch between local excited state and charge transfer state. Crystallographic study indicates that the bulky structure and weak intermolecular interactions account for polymorphism and AIE properties. This work will provide a simple molecular design strategy for multifunctional materials.

* Corresponding author.

** Corresponding author.

E-mail addresses: huangbinhb31@sina.com (B. Huang), guning@seu.edu.cn (N. Gu).¹ These authors contributed equally to this work.

1. Introduction

Luminescent materials based on purely organic compounds have received raising attention in recent years for various applications ranging from chemical sensors, biomedicine, to light-emitting devices etc [1, 2, 3, 4, 5, 6, 7]. Based on the luminescent features, luminescent materials can be classified into aggregation-induced emission (AIE) luminogens, mechanochromic luminescent (MCL) fluorophores, thermally activated delayed fluorescence (TADF) emitters or their combination. AIE luminogens are compounds that show negligible emission in dilute solution while intense luminescence in solid state. In principle, AIE is attributed to the restriction of free intramolecular rotations and vibrations in aggregation state [8, 9, 10]. AIE-active compounds can serve as efficient emitters in light-emitting devices and as photosensitizers in biomedical field [11, 12, 13]. Interestingly, MCL fluorophores are compounds that exhibit reversible emission color change upon external stimuli (e.g. grinding, pressing, rubbing, heating, organic vapor treatments etc) [14, 15, 16, 17, 18]. Due to their unique features, MCL emitters can be applied in stress-, pressure-, and thermo-indicators in the future [19, 20, 21]. In the past ten years, great efforts have been made to develop TADF emitters, which possess small energy splits (ΔE_{STs}) between singlet (S_1) and triplet (T_1) excited states to facilitate upconversion from T_1 to S_1 through reverse intersystem crossing (RISC) [22, 23, 24, 25, 26]. TADF emitters have aroused increasing interest for their promising implications in optoelectronic and biomedical fields [27, 28, 29, 30].

Nowadays, compared with single-function (AIE, MCL or TADF) emitting materials, multifunctional emitting materials offer more opportunities in practical applications [31, 32, 33, 34, 35]. The development of multifunctional materials have attracted more and more attention. In 2015, Chi's group reported the first multifunctional material 4-carbazol-10-phenothiazine diphenyl sulfone that shows AIE, TADF, and MCL properties simultaneously [36]. In 2017, Takeda et al developed a series TADF molecules based on phenothiazine-dibenzo[*a,j*]phenazine-phenothiazine with multi-color-changing MCL properties [37]. Our group also reported a series of AIE-TADF-MCL emitters based on donors substituted anthraquinone [38, 39]. Yang's group reported two

mulfifunctional emitters based on quinoxaline with simultaneous polymorph-dependent TADF, AIE, and multi-color MCL features [40]. However, to date, multifunctional emitting materials are limited in number and need to be further explored. The development of a simple molecular design for combining AIE, TADF and MCL properties in a single compound is highly desired.

Our group previously reported a series of MCL-active isomers by employing triphenylamine (TPA) and benzo[*d,e*]benzo [4,5]imidazo[2, 1-*a*]isoquinolin-7-one (BBI) as the electron donor and acceptor, respectively [41, 42]. Due to the change of $\pi\text{-}\pi$ interactions in different aggregation states, these isomers show high-contrast MCL property. However, these compounds have large overlaps between the highest occupied molecular orbital (HOMO) and the lowest unoccupied molecular orbital (LUMO), leading to large ΔE_{STs} (>0.5 eV) and no TADF features. In this report, we attempted to provide a simple molecular design strategy towards the conversion of a MCL skeleton to a multifunctional emitter. Through altering the substituent sites and increasing the number of TPA moieties and steric hindrance on the MCL building block BBI, a novel multifunctional material 10,11-bis(4-diphenylamino-phenyl)-benzo[*d,e*]benzo [4,5]imidazo[2,1-*a*]isoquinolin-7-one (10, 11-2TPA-BBI, Figure 1) is successfully synthesized. Due to the change of substituent sites and the increase of electron-donating TPA moieties, the overlap between HOMO and LUMO is significantly decreased, inducing a small ΔE_{ST} of 0.19 eV. Interestingly, 10,11-2TPA-BBI can form four different aggregate species: yellow solid (YS), orange solid (OS), orange flake-shaped crystal (OC), and red prism-like crystal (RC). Among the four aggregates, OS, OC and RC exhibit TADF properties, while YS show normal fluorescence characteristics. Under external stimuli, OS can be reversibly switched to YS, indicating MCL property. Because of the increased steric hindrance, there are no strong $\pi\text{-}\pi$ interactions in OC or RC. The weak interactions in the crystals are conducive to inhibiting intramolecular rotations, which may help to explain the AIE property of the compound. We believe that the conversion of a normal MCL backbone to a multifunctional emitter would be a significantly powerful strategy for creating multifunctional organic materials.

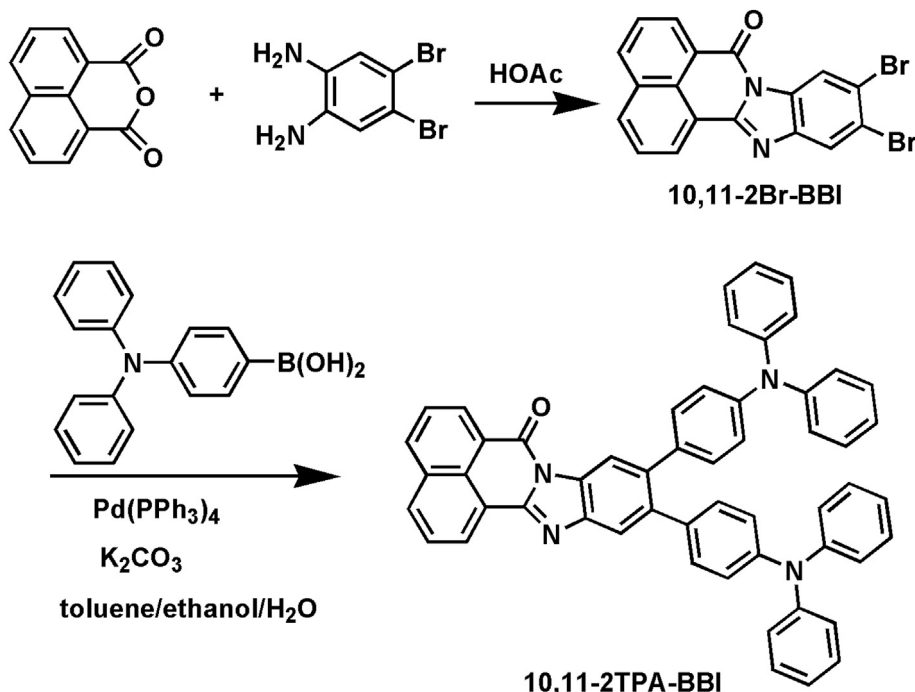


Figure 1. Synthesis route of 10,11-2TPA-BBI.

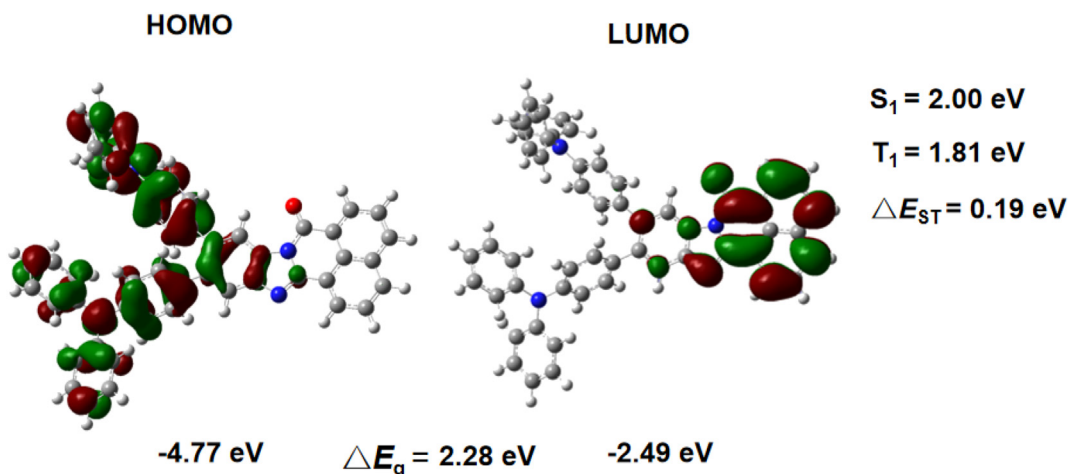


Figure 2. Calculated energy levels for 10,11-2TPA-BBI.

2. Experimental

2.1. Chemicals and instruments

The reagents (analytical grade) and solvents (HPLC grade) were purchased from Aladdin Bio-chem Technology Co., LTD (Shanghai, China) and used as received. Mass spectra was performed using a mass spectrometer (Finnigan LTQ, Thermo Electron Corporation). ^1H and ^{13}C NMR spectrum of the target compound were measured in CDCl_3 on a NMR spectrometer (Bruker AV 400 M) with tetramethylsilane as the internal standard. UV-vis absorption spectrum were performed in the range of 260–600 nm in Agilent 8453 UV-vis spectrophotometer. The photoluminescence spectra (PL), phosphorescence spectra (PH), photoluminescence quantum yield (ϕ_{PL}) and transient PL lifetimes of the samples were measured using a spectrophotometer (Edinburgh FLS 980). The powder X-ray diffraction (XRD) measurements of the samples were collected on a diffractometer (Ultima IV) with $\text{Cu-K}\alpha$ radiation at a scan rate of 2° min^{-1} [20]. Single crystal XRD measurements of the crystals were carried out using Oxford Gemeni S Ultra X-ray diffractometer with $\text{Mo-K}\alpha$ radiation at 296 K. CCDC 2034918 (RC) and 2034919 (OC) contain the supplementary crystallographic data for this paper [43].

The molecular structure, HOMO and LUMO of 10,11-2TPA-BBI were optimized by density functional theory (DFT) calculations at B3LYP/6-31G(d) level (Gaussian 09 program package) [44]. Based on the optimized geometry of 10,11-2TPA-BBI at ground state, the excitation energies were calculated by time-dependent density functional theory (TD-DFT) method [45].

2.2. Synthesis of the target molecule

2.2.1. Synthesis of 10,11-dibromo-benzo[d,e]benzo[4,5]imidazo[2,1-a]isoquinolin-7-one (10,11-2Br-BBI)

In a 250 mL three-necked flask, 1,8-naphthalic anhydride (6.0 mmol) and 4,5-dibromo-1,2-benzenediamine (6.0 mmol) were added to 100 mL glacial CH_3COOH . The mixture was refluxed for 6 h. After cooling, 100

Table 1. Calculated triplet and singlet excitation energies (vertical transition), oscillator strength (f), transition probability (p), and transition configurations of 10,11-2TPA-BBI.

state	E (eV)	f	main configuration	p	ΔE_{ST} (eV)
S_1	2.00	0.343	$\text{H} \rightarrow \text{L}$	0.71	0.19
S_2	2.16	0.216	$\text{H} \rightarrow \text{L}$	0.69	
T_1	1.81	0	$\text{H} \rightarrow \text{L}$	0.53	
T_2	2.09	0	$\text{H} \rightarrow \text{L}$	0.42	

mL deionized water was added. The yellow precipitate was filtered, dried, and used for the preparation of 10,11-2TPA-BBI without purification (yield >95%).

2.2.2. Synthesis of 10,11-2TPA-BBI

In a 250 mL three-necked flask, a mixture of 10,11-2Br-BBI (4.0 mmol), 4-(diphenylamino)phenyl boronic acid (8.8 mmol) in toluene (60 mL), ethanol (30 mL) and aqueous potassium carbonate solution (1.0 M, 20 mL) was stirred under N_2 for 10 min. After the addition of tetrakis-triphenylphosphine)palladium (0.4 mmol), the mixture was refluxed under nitrogen for 18 h. Cooling to room temperature, 80 mL deionized water was added. The mixture was extracted with 100 mL dichloromethane (DCM) for two times. Then the organic phase was combined, washed with saturated aqueous sodium chloride solution (2×40 mL), dried over anhydrous sodium sulfate, and concentrated under vacuum. The crude product was purified by column chromatography (silica gel; eluent: 10% ethyl acetate/petroleum ether) to give 10,11-2TPA-BBI as an orange solid with a yield of 70.4%. ^1H NMR (400 MHz, CDCl_3) δ (ppm): 8.92 (d, $J = 8.0$ Hz, 1H), 8.84 (d, $J = 8.0$ Hz, 1H), 8.66 (s, 1H), 8.33 (d, $J = 8.0$ Hz, 1H), 8.21 (d, $J = 8.0$ Hz, 1H), 7.97 (s, 1H), 7.88–7.84 (m, 2H), 7.37–7.29 (m, 8H), 7.20–7.15 (m, 12H), 7.08–7.04 (m, 8H). ^{13}C NMR (100 MHz, CDCl_3) δ (ppm): 160.66, 149.90, 147.76, 146.36, 143.15, 138.85, 138.64, 136.05, 135.86, 135.37, 132.31, 131.89, 131.73, 131.20, 131.17, 131.06, 129.28, 127.42, 127.25, 126.95, 124.37, 124.27, 123.24, 123.20, 123.05, 122.81, 122.75, 120.94, 120.74, 117.10. MS (MALDI-TOF) [m/z]: Calcd for $\text{C}_{54}\text{H}_{36}\text{N}_4\text{O}$, 756.87; Found: 756.95.

2.3. Different aggregates of 10,11-2TPA-BBI

The as-prepared 10,11-2TPA-BBI sample is OS, while OS can be converted to YS form upon heating at 170°C for 5 s. At room temperature, OC and RC of 10,11-2TPA-BBI were grown from methanol/DCM (v:v = 1:1) and ethanol/chloroform (v:v = 1:1) solution by slow evaporation, respectively.

3. Results and discussion

3.1. Synthesis

Synthetic route of 10,11-2TPA-BBI is illustrated in Figure 1. First, the key intermediate 10,11-2Br-BBI is synthesized by condensation reaction of 1,8-naphthalic anhydride with 4,5-dibromo-1,2-benzenediamine. Then 10,11-2Br-BBI is transformed into the target compound 10,11-2TPA-BBI by Suzuki reaction with 4-(diphenylamino)phenyl boronic acid. The structure of 10,11-2TPA-BBI is confirmed by MS, ^1H NMR, ^{13}C NMR, and single-crystal measurements.

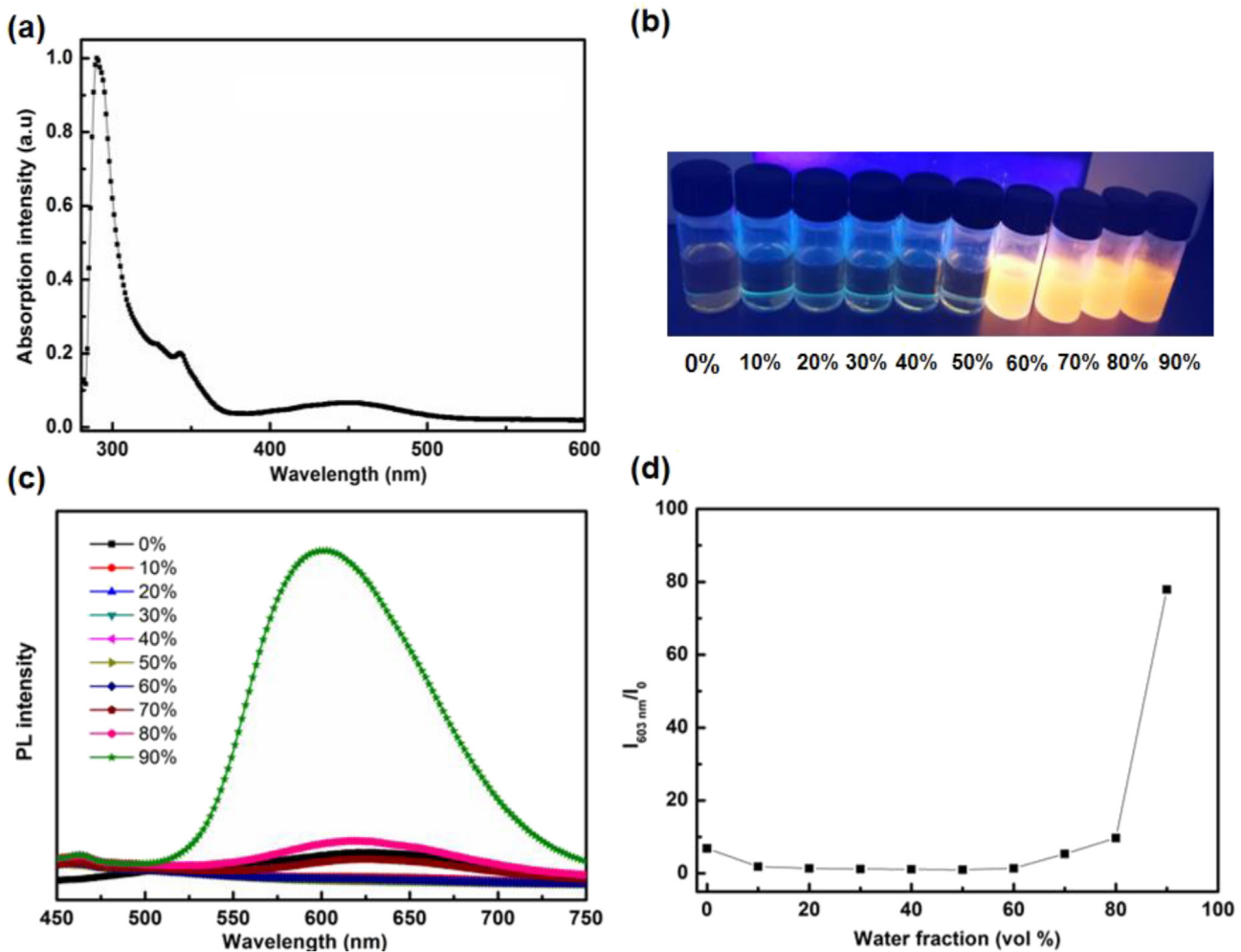


Figure 3. (a) UV-vis absorption spectra of 10, 11-2TPA-BBI in toluene; (b) The digital photographs of 10,11-2TPA-BBI in THF/water mixtures with different water fractions under 365 nm UV excitation; (c) PL spectra of 10,11-2TPA-BBI in THF/water mixtures with different water fractions; (d) Plot of $I_{603 \text{ nm}} / I_0$ versus water content of the solvent mixture, where I_0 is the PL intensity of 10,11-2TPA-BBI in pure THF solution.

3.2. Theoretical calculations

To optimize the geometry and predict the HOMO and LUMO electronic distributions of 10,11-TPA-BBI, DFT calculations were performed. As shown in Figure 2, the HOMO of 10,11-TPA-BBI is mainly localized over the TPA units, while the LUMO is dispersed on the BBI moiety. The HOMO and LUMO energy levels of 10,11-TPA-BBI are estimated to be -4.77 eV and -2.49 eV, respectively. Accordingly, the optical bandgap (E_g) is calculated to be 2.28 eV, which is smaller than the reported MCL emitters based on TPA substituted BBI (3-TPA-BBI and 4-TPA-BBI) [41, 42], indicating the increase of molecular conjugation. Compared with 3-TPA-BBI and 4-TPA-BBI, the overlap between HOMO and LUMO of 10,11-TPA-BBI is significantly decreased, which can be attributed to the change of the substituent sites and the increase of the number of TPA moieties. Based on the optimized geometries, TD-DFT calculations were performed to predict the ΔE_{ST} of 10,11-TPA-BBI. As expected, the small overlap between HOMO and LUMO leads to a small ΔE_{ST} of 0.19 eV (Table 1), which is much smaller than 3-TPA-BBI and 4-TPA-BBI [41, 42]. The small ΔE_{ST} indicates that 10,11-TPA-BBI may serve as a typical TADF emitter.

3.3. Spectroscopic properties of 10,11-2TPA-BBI in solvents

UV-vis absorption spectrum of 10,11-2TPA-BBI in toluene is presented in Figure 3a. The absorption profile of 10,11-2TPA-BBI consists of three absorption band regions. The two bands at around 300 and 340 nm are attributed to the $\pi-\pi^*$ and $n-\pi^*$ transitions, respectively, while the

longer-wavelength absorption at around 450 nm belongs to intramolecular charge transfer (ICT) from TPA moieties to BBI unit. From the onset absorption (520 nm), E_g of 10,11-2TPA-BBI can be calculated to be 2.38 eV, which is in good agreement with the above-mentioned theoretical result (2.28 eV).

PL spectra of 10,11-2TPA-BBI in solution are also investigated. As illustrated in Figure 3b-c, 10,11-2TPA-BBI exhibits faint emission in tetrahydrofuran (THF) solution. With the addition of deionized water fraction (f_w), the PL intensity of 10,11-2TPA-BBI first decreases and then enhances gradually. The decrease of PL intensity at low f_w (10%) can be attributed to the slight increase of solvent polarity, which is in favor of molecular motions and non-radiative decay. With f_w increases to 60%, the aggregates may form and restrict intramolecular motions, and thus inhibit non-radiative decay and increase PL intensity. When f_w increases to 90%, the fluorescence intensity reaches to 80-fold of that in pure THF solution, indicating the typical AIE feature of 10,11-2TPA-BBI (Figure 3d) [33]. Note that the reported BBI based compounds 3-TPA-BBI and 4-TPA-BBI are not AIE-active [41, 42]. This verifies that the change of the substituent sites and the increase of the number of TPA moieties are beneficial for restricting intramolecular motions and induce AIE property.

3.4. Polymorphism and TADF properties of 10,11-2TPA-BBI in aggregation states

Through controlling the preparation conditions mentioned above, 10,11-2TPA-BBI formed four different aggregates: YS, OS, OC and RC

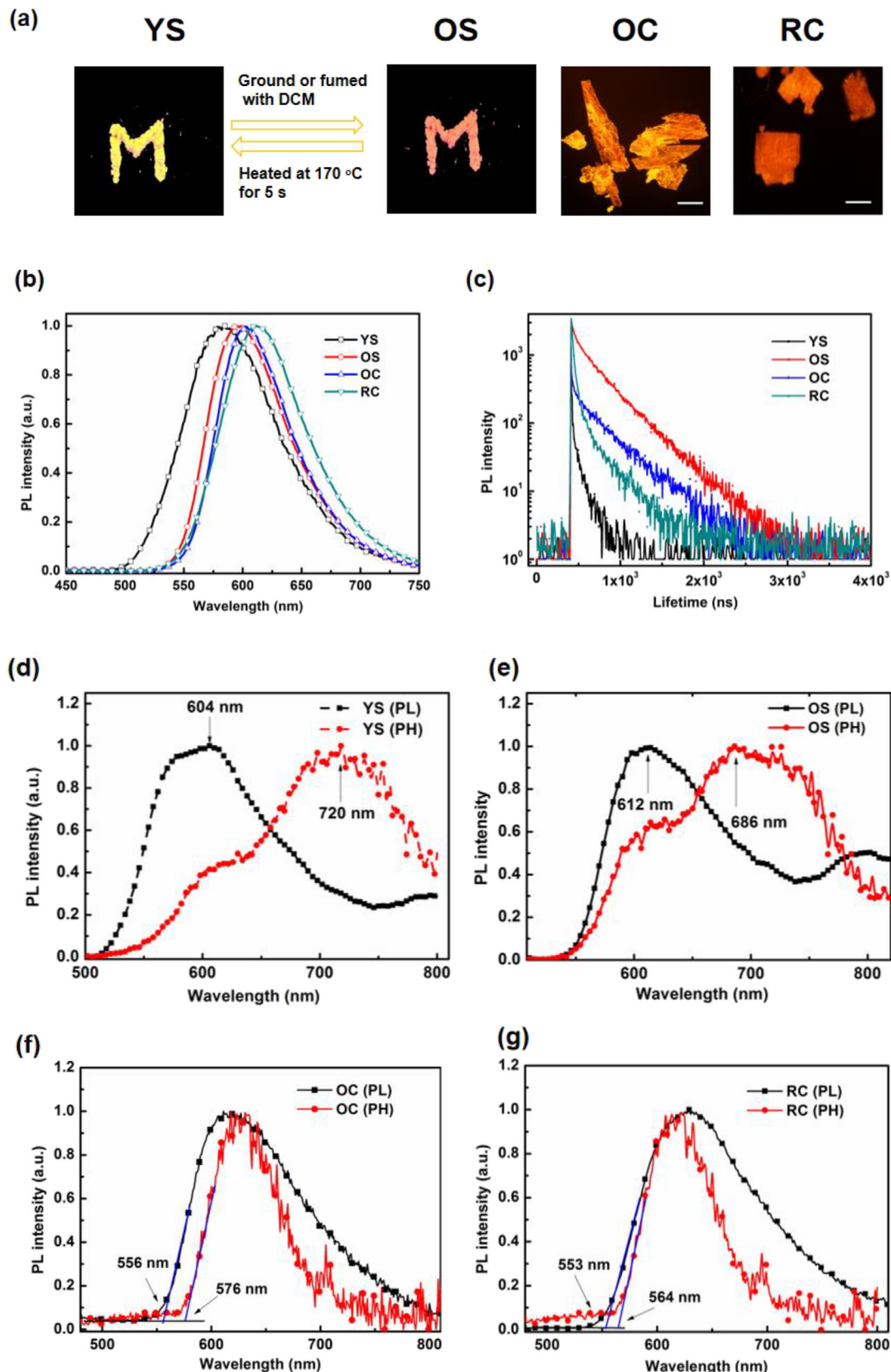


Figure 4. (a) Photographs of the four solid states of 10,11-2TPA-BBI under the 365 nm UV excitation (a letter “M” based on YS or OS; scale bar: 1 mm); (b) PL spectra of 10,11-2TPA-BBI in different aggregation states; (c) PL decay curves of 10,11-2TPA-BBI in different aggregation states; The time-resolved PL and PH spectra of 10,11-2TPA-BBI in different aggregation states with 1 ms delay at 77 K: (d) YS; (e) OS; (f) OC; (g) RC.

Table 2. PL characteristics of 10,11-2TPA-BBI in solid states.

	YS	OS	OC	RC
λ_{PL} (nm)	583	598	603	613
Φ_{PL}	0.148	0.154	0.281	0.205
τ_p (ns)	60.36 (100%)	61.42 (13.65%)	5.80 (12.27%)	10.00 (30.18%)
τ_d (μ s)	/	0.34 (86.35%)	0.35 (87.73%)	0.15 (69.82%)
k_r (10^7 s $^{-1}$)	0.25	0.25	4.84	2.05
k_{nr} (10^7 s $^{-1}$)	1.41	1.38	12.40	7.95
S_1 (eV)	2.05 (1 LE)	2.03 (1 CT)	2.23 (1 CT)	2.24 (1 CT)
T_1 (eV)	1.72 (3 LE)	1.81 (3 LE)	2.15 (3 CT)	2.20 (3 CT)
ΔE_{ST} (eV)	0.33	0.22	0.08	0.04

(Figure 4a). As illustrated in Figure 4b and Table 2, the four aggregates of 10,11-2TPA-BBI exhibit PL spectra with emission peaks at 583 nm (YS), 598 nm (OS), 602 nm (OC) and 610 nm (RC), respectively. The results indicate that different aggregates have important effects on the PL spectra, reflecting different molecular conformations or intermolecular interactions [39]. To better investigate the PL property of 10,11-2TPA-BBI, Φ_{PL} values of the four aggregates are obtained to be 0.148 (YS), 0.154 (OS), 0.281 (OC) and 0.205 (RC), respectively (Table 2). OC and RC have larger Φ_{PL} values than YS and OS, suggesting that crystalline state is beneficial for radiative decay.

To confirm the TADF properties of 10,11-2TPA-BBI, we measured the transient PL decay of four aggregates at room temperature. As illustrated in Figure 4c, the transient PL decays of OS, OC and RC are all composed of prompt fluorescence in the nanosecond range and delayed fluorescence in the microsecond range, reflecting typical TADF characteristics [46]. In contrast, YS only show prompt fluorescence in the nanosecond range with a lifetime of 60.36 ns, suggesting normal fluorescence characteristics. The prompt/delayed fluorescence lifetime (τ_p/τ_d) values are 61.42 ns/0.34 μ s for OS, 5.80 ns/0.35 μ s for OC, and 10.0 ns/0.15 μ s for RC, respectively. To further understand the influence of aggregation state on the fluorescence decay process, radiative and non-radiative decay rate constants ($k_r = \Phi_{PL}/\tau_p$, $k_{nr} = (1-\Phi_{PL})/\tau_p$) are calculated (Table 2), respectively. In the case of YS and OS, the small k_r value (0.25×10^7 s $^{-1}$) may be attributed to the disordered amorphous state, which may inhibit radiative transition. In contrast, OC exhibits the largest k_r value of 4.84×10^7 s $^{-1}$, suggesting that a large k_r can be realized in the crystalline state via modulation of intermolecular interactions.

Next, we examined time-resolved PL and PH spectra of these aggregates with 1 m delay at 77 K. The results are illustrated in Figure 4d-g and Table 2. YS exhibits finely structured PL and PH spectra, which ascribe to the local excited (LE) state [47]. In contrast, OS shows broad PL

and finely structured PH, corresponding to charge transfer (CT) excited state and LE state, respectively [47]. In the case of OC and RC, broad PL and PH spectra reflect the CT excited states in crystals. From the PL spectra, the S_1 energy values of the four aggregates are calculated to be 2.05 eV (YS), 2.03 eV (OS), 2.23 eV (OC) and 2.24 eV (RC). From the PH spectra at 77 K, T_1 energy values are estimated to be 1.72 eV (YS), 1.81 eV (OS), 2.15 eV (OC) and 2.20 eV (RC), respectively. Correspondingly, ΔE_{STS} are obtained to be 0.33 eV (YS), 0.22 eV (OS), 0.08 eV (OC) and 0.04 eV (RC). Note that OS, OC and RC have small ΔE_{STS} (<0.3 eV), which facilitate upconversion from T_1 to S_1 state through RISC and induce TADF emission. In contrast, YS has a larger ΔE_{STS} (>0.3 eV) and shows no TADF behavior.

3.5. MCL property of 10,11-2TPA-BBI

Among the four aggregates, OS can be transformed into YS upon heating (170 °C, 5 s), and YS can be converted back to OS form via grinding or fuming with DCM vapor (Figure 4a). Upon external stimuli, the reversible conversion between OS and YS indicates typical MCL property of 10,11-2TPA-BBI. By comparing the PL spectra of YS and OS at 77 K (Figure 4d-e), the MCL behavior of 10,11-2TPA-BBI can be attributed to the emission switch between LE (YS) and CT (OS). The XRD patterns of the four aggregates are shown in Figure 5a, YS and OS show no evident diffraction peaks, indicating that YS and OS are both in amorphous states. In contrast, OC and RC exhibit strong and evident diffraction peaks, suggesting the ordered structures of OC and RC.

Figure 5b shows the maximum PL emission of 10,11-2TPA-BBI upon being treated by heating (or grinding) and fuming with DCM, indicating that the transformation between YS and OS upon external stimulus has good repeatability. Note that the emission color change of 10,11-2TPA-BBI during MCL process is smaller than 3-TPA-BBI and 4-TPA-BBI, in which MCL property may originate from different π - π interactions of the aggregates [41, 42]. In the case of 10,11-2TPA-BBI, it is difficult for the molecules to form π - π stacking in these aggregates because of the bulky structure.

3.6. Single crystallographic analysis of 10,11-2TPA-BBI

To investigate the influence of crystal structures on photophysical properties, the single-crystal analysis of OC and RC were conducted. The details of the structures were summarized in Figure 6a-b and Table 3. OC is triclinic with space group of P-1. In contrast, RC is monoclinic with space group of P2₁/c. The formulas of OC and RC are C₁₀₉H₇₃Cl₃N₈O₂ (the solvent chloroform and 10,11-2TPA-BBI with a ratio of 1:2) and C₅₆H₄₄N₄O₃ (the solvent methanol and 10,11-2TPA-BBI with a ratio of

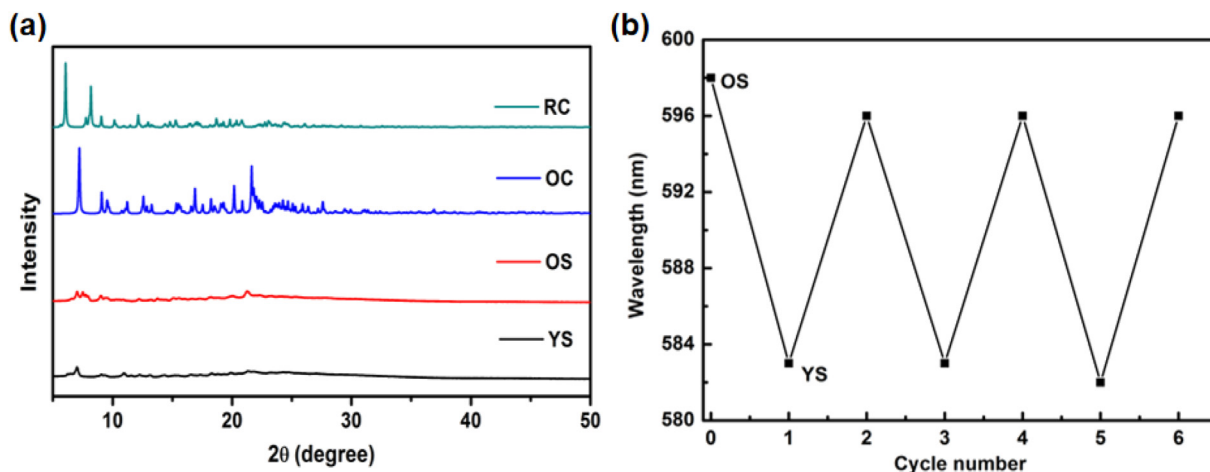


Figure 5. (a) XRD spectra of 10,11-2TPA-BBI in different solid states; (b) maximum PL emission of 10,11-2TPA-BBI upon being treated by heating (or grinding) and fuming with DCM.

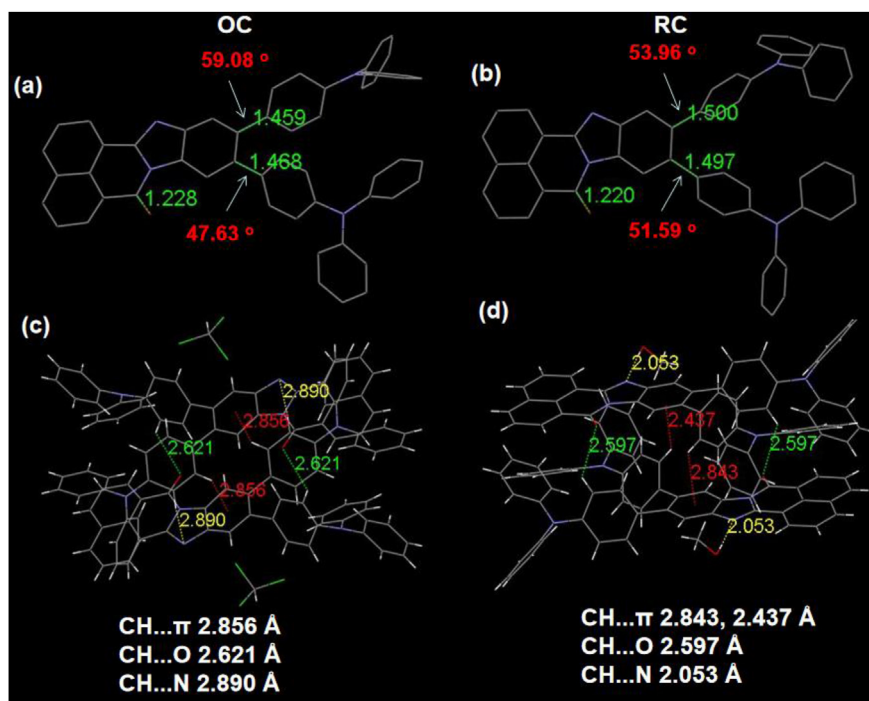


Figure 6. The single crystal structures (hydrogen atoms have been omitted for clarity) of OC (a) and RC (b); molecular interactions of OC (c) and RC (d).

2:1), respectively. As expected, both crystals exhibit twisted molecular structures. In these crystals, the dihedral angles between BBI plane and the neighbouring phenyl planes of TPA units are 59.08/47.63° (OC) and 53.96/51.59° (RC). The corresponding bond lengths are 1.459/1.468 Å (OC) and 1.500/1.497 Å (RC), respectively. The bond lengths of C=O are 1.228 Å (OC) and 1.220 Å (RC) (Figure 5a-b). Compared with OC, RC exhibits similarly twisted conformation but longer bond lengths between

electron-donating TPA moieties and electron-accepting BBI unit, indicating that the conjugation is increased in RC. The results are consistent with the red-shifted PL spectra of RC comparing to OC (Figure 3b).

As a step further to investigate the different luminous properties of OC and RC, the intermolecular interactions in the crystals were analyzed (Figure 6c-d). Due to the twisted conformations and bulky structures, the 10,11-2TPA-BBI molecules couldn't form intermolecular aromatic packing, leading to no strong intermolecular interactions such as $\pi\cdots\pi$ interactions in OC or RC. In the case of OC, two 10,11-2TPA-BBI molecules form a pair by C-H \cdots π, C-H \cdots O and C-H \cdots N intermolecular interactions with distances of 2.856 Å, 2.621 Å and 2.890 Å, respectively. Note that there is no obvious intermolecular interactions between 10,11-2TPA-BBI molecules and the adjacent chloroform molecules. In contrast, the neighbouring 10,11-2TPA-BBI molecules are bound by C-H \cdots π and C-H \cdots O intermolecular interactions distances of 2.843/2.437 Å and 2.597 Å in RC. In addition, there is C-H \cdots N intermolecular interactions with distances of 2.053 Å between methanol molecules and the adjacent 10,11-2TPA-BBI molecules. Compared with OC, the shortened C-H \cdots π, C-H \cdots O and C-H \cdots N distances in RC indicate that intermolecular interactions are enhanced, which also contribute to the red-shifted PL spectra of RC versus OC [48]. Meanwhile, the weak intermolecular interactions in the single crystals are conducive to restraining intramolecular rotations, which may help to explain the AIE property of 10, 11-2TPA-BBI.

4. Conclusions

In summary, we successfully converted a MCL-active backbone BBI to a multifunctional emitter 10,11-2TPA-BBI by molecular modification. As expected, the compound exhibits polymorphism, AIE, MCL and TADF properties simultaneously. TADF is achieved by altering the substituent sites and increasing the number of electron-donating TPA moieties on the electron-accepting BBI unit. PL emission switch between LE and CT states is responsible for the MCL behavior. The bulky structure and weak intermolecular interactions contribute to polymorphism and AIE properties. In all, the current work demonstrated a simple molecular design strategy towards the conversion of a MCL backbone to a multifunctional

Table 3. Crystal data and structure refinement for 10,11-2TPA-BBI.

	OC	RC
Formula	C ₁₀₉ H ₇₃ Cl ₃ N ₈ O ₂	C ₅₆ H ₄₄ N ₄ O ₃
CCDC No.	2034919	2034918
Formula weight	1633.10	820.95
Space group	P-1	P2 ₁ /c
Temperature	296	296
Wavelength/Å	0.71073	0.71073
Crystal system	Triclinic	Monoclinic
a/Å	13.267(2)	12.428(9)
b/Å	16.259(3)	14.064(10)
c/Å	22.397(3)	25.185(18)
$\alpha/^\circ$	74.897(6)	90.000
$\beta/^\circ$	85.589(7)	101.955(9)
$\gamma/^\circ$	84.927(7)	90.000
Volume/Å ³	4639.0(13)	4307.0(5)
Z	2	4
Calculated density/Mg m ⁻³	1.169	1.360
M(mm ⁻¹)	0.153	0.079
F(000)	1700	1728
Crystal size/mm ³	0.15 × 0.18 × 0.20	0.14 × 0.15 × 0.18
No. of reflns collected	16104	7678
No. of unique reflns	4523	4430
Goodness-of-fit on F ²	0.920	1.266
R ₁ , wR ₂ [$I > 2\sigma(I)$]	0.1047, 0.2251	0.0734, 0.2066
R ₁ , wR ₂ (all data)	0.2762, 0.2671	0.1308, 0.2359

emitter, which would provide a guideline for the design of multifunctional materials.

Declarations

Author contribution statement

Bin Huang: Conceived and designed the experiments; Contributed reagents, materials, analysis tools or data; Wrote the paper.

Wenbing Yu, Li Yang: Performed the experiments.

Yan Li: Analyzed and interpreted the data; Contributed reagents, materials, analysis tools or data.

Ning Gu: Conceived and designed the experiments; Wrote the paper.

Funding statement

This work was supported by Postdoctoral Research Foundation of China (2020M681464), Jiangsu Planned Projects for Postdoctoral Research Funds (2021K601C), Natural Science Research of Jiangsu Higher Education Institutions of China (19KJB150006), National Key Research and Development Program of China (2017YFA0104302) and National Natural Science Foundation of China (51832001, 61821002).

Data availability statement

Data included in article/supplementary material/referenced in article.

Declaration of interests statement

The authors declare no conflict of interest.

Additional information

Supplementary content related to this article has been published online at <https://doi.org/10.1016/j.heliyon.2022.e11221>

References

- [1] J. Chan, S.C. Dodani, C.J. Chang, Reaction-based small-molecule fluorescent probes for chemoselective bioimaging, *Nat. Chem.* 4 (2012) 973–984.
- [2] T. Yoshii, K. Mizusawa, Y. Takaoka, I. Hamachi, Intracellular protein-responsive supramolecules: protein sensing and in-cell construction of inhibitor assay system, *J. Am. Chem. Soc.* 136 (2014) 16635–16642.
- [3] J. Wu, B. Kwon, W. Liu, E.V. Anslyn, P. Wang, J.S. Kim, Chromogenic/fluorogenic ensemble chemosensing systems, *Chem. Rev.* 115 (2015) 7893–7943.
- [4] X. Chen, F. Wang, J.Y. Hyun, T. Wei, J. Qiang, X. Ren, I. Shin, J. Yoon, Recent progress in the development of fluorescent, luminescent and colorimetric probes for detection of reactive oxygen and nitrogen species, *Chem. Soc. Rev.* 45 (2016) 2976–3016.
- [5] V.-N. Nguyen, Y. Yan, J. Zhao, J. Yoon, Heavy-atom-free photosensitizers: from molecular design to applications in the photodynamic therapy of cancer, *Acc. Chem. Res.* 54 (2021) 207–220.
- [6] X. Zhao, J. Liu, J. Fan, H. Chao, X. Peng, Recent progress in photosensitizers for overcoming the challenges of photodynamic therapy: from molecular design to application, *Chem. Soc. Rev.* 50 (2021) 4185–4219.
- [7] Z. Yang, Z. Mao, Z. Xie, Y. Zhang, S. Liu, J. Zhao, J. Xu, Z. Chi, M.P. Aldred, Recent advances in organic thermally activated delayed fluorescence materials, *Chem. Soc. Rev.* 46 (2017) 915–1016.
- [8] J. Luo, Z. Xie, J.W.Y. Lam, L. Cheng, B.Z. Tang, H. Chen, C. Qiu, H.S. Kwok, X. Zhan, Y. Liu, D. Zhu, Aggregation-induced emission of 1-Methyl-1,2,3,4,5-pentaphenylsilole, *Chem. Commun.* 18 (2001) 1740–1741.
- [9] Y. Hong, J.W.Y. Lam, B.Z. Tang, Aggregation-induced emission, *Chem. Soc. Rev.* 40 (2011) 5361–5388.
- [10] J. Mei, N.L. Leung, R.T. Kwok, J.W. Lam, B.Z. Tang, Aggregation-induced emission: together we shine, united we soar, *Chem. Rev.* 115 (2015) 11718–11940.
- [11] T. Zhang, Q. Peng, C. Quan, H. Nie, Y. Niu, Y. Xie, Z. Zhao, B.Z. Tang, Z. Shuai, Using the isotope effect to probe an aggregation induced emission mechanism: theoretical prediction and experimental validation, *Chem. Sci.* 7 (2016) 5573–5580.
- [12] Z. Zhao, H. Zhang, J.W.Y. Lam, B.Z. Tang, Aggregation-induced emission: new vistas at the aggregate level, *Angew. Chem. Int. Ed.* 59 (2020) 9888–9907.
- [13] H. Chen, Y. Wan, X. Cui, S. Li, C.-S. Lee, Recent advances in hypoxia-overcoming strategy of aggregation-induced emission photosensitizers for efficient photodynamic therapy, *Adv. Healthcare Mater.* 10 (2021) 2101607.
- [14] Y. Sagara, T. Kato, Mechanically induced luminescence changes in molecular assemblies, *Nat. Chem.* 1 (2009) 605–610.
- [15] Z. Chi, X. Zhang, B. Xu, X. Zhou, C. Ma, Y. Zhang, S. Liu, J. Xu, Recent advances in organic mechanofluorochromic materials, *Chem. Soc. Rev.* 41 (2012) 3878–3896.
- [16] K. Isayama, N. Aizawa, J.Y. Kim, T. Yasuda, Modulating photo- and electroluminescence in a stimuli-responsive π-conjugated donor-acceptor molecular system, *Angew. Chem. Int. Ed.* 57 (2018) 11982–11986.
- [17] J. Yang, J. Qin, P. Geng, J. Wang, M. Fang, Z. Li, Molecular conformation-dependent mechanoluminescence: same mechanical stimulus but different emissive color over time, *Angew. Chem., Int. Ed.* 57 (2018) 16407–16411.
- [18] K. Isayama, N. Aizawa, J.Y. Kim, T. Yasuda, Modulating photo- and electroluminescence in a stimuli-responsive π-conjugated donor-acceptor molecular system, *Angew. Chem. Int. Ed.* 57 (2018) 11982–11986.
- [19] S. Hirata, T. Watanabe, Reversible thermoresponse recording of fluorescent images (TRF), *Adv. Mater.* 18 (2006) 2725–2729.
- [20] M. Kinami, B.R. Crenshaw, C. Weder, Polyesters with built-in threshold temperature and deformation sensors, *Chem. Mater.* 18 (2006) 946–955.
- [21] A. Pucci, F. Di Ciaia, F. Signori, G. Ruggeri, Bis(benzoxazolyl)stilbene excimers as temperature and deformation sensors for biodegradable poly(1,4-butylene succinate) films, *J. Mater. Chem.* 17 (2007) 783–790.
- [22] H. Uoyama, K. Goushi, K. Shizu, H. Nomura, C. Adachi, Highly efficient organic light-emitting diodes from delayed fluorescence, *Nature* 492 (2012) 234–240.
- [23] Y. Tao, K. Yuan, T. Chen, P. Xu, H. Li, R. Chen, C. Zheng, L. Zhang, W. Huang, Thermally activated delayed fluorescence materials towards the breakthrough of organoelectronics, *Adv. Mater.* 26 (2014) 7931–7958.
- [24] Y.J. Cho, K.S. Yook, J.Y. Lee, High efficiency in a solution-processed thermally activated delayed fluorescence device using a delayed fluorescence emitting material with improved solubility, *Adv. Mater.* 26 (2014) 6642–6646.
- [25] S. Hirata, Y. Sakai, K. Masui, H. Tanaka, S.Y. Lee, H. Nomura, N. Nakamura, M. Yasumatsu, H. Nakamoto, Q.S. Zhang, K. Shizu, H. Miyazaki, C. Adachi, Highly efficient blue electroluminescence based on thermally activated delayed fluorescence, *Nat. Mater.* 14 (2015) 330–336.
- [26] Q. Zhang, B. Li, S. Huang, H. Nomura, H. Tanaka, C. Adachi, Efficient blue organic light-emitting diodes employing thermally activated delayed fluorescence, *Nat. Photonics* 8 (2014) 326–332.
- [27] D. Zhang, M. Cai, Y. Zhang, D. Zhang, L. Duan, Sterically shielded blue thermally activated delayed fluorescence emitters with improved efficiency and stability, *Mater. Horiz.* 3 (2016) 145–151.
- [28] D. Chen, K. Liu, L. Gan, M. Liu, K. Gao, G. Xie, Y. Ma, Y. Cao, S.J. Su, Modulation of exciton generation in organic active planar p-n heterojunction: toward low driving voltage and high-efficiency OLEDs employing conventional and thermally activated delayed fluorescent emitters, *Adv. Mater.* 28 (2016) 6758–6765.
- [29] F. Ni, Z. Zhu, X. Tong, W. Zeng, K. An, D. Wei, S. Gong, Q. Zhao, X. Zhou, C. Yang, Hydrophilic, red-emitting, and thermally activated delayed fluorescence emitter for time-resolved luminescence imaging by mitochondrion-induced aggregation in living cells, *Adv. Sci.* 6 (2019), 1801729.
- [30] F. Fang, L. Zhu, M. Li, Y. Song, M. Sun, D. Zhao, J. Zhang, Thermally activated delayed fluorescence material: an emerging class of metal-free luminophores for biomedical applications, *Adv. Sci.* 8 (2021), 2102970.
- [31] P. Data, Y. Takeda, Recent advancements in and the future of organic emitters: TADF- and RTP-active multifunctional organic materials, *Chem. Asian J.* 14 (2019) 1613–1636.
- [32] H. Yu, X. Song, N. Xie, J. Wang, C. Li, Y. Wang, Reversible crystal-to-crystal phase transitions with high-contrast luminescent alterations for a thermally activated delayed fluorescence emitter, *Adv. Funct. Mater.* 31 (2021), 2007511.
- [33] K. Zheng, H. Yang, F. Ni, Z. Chen, S. Gong, Z. Lu, C. Yang, Multifunctional thermally activated delayed fluorescence emitters and insight into multicolor-mechanochromism promoted by weak intra- and intermolecular interactions, *Adv. Opt. Mater.* 7 (2019), 1900727.
- [34] K. Zhang, Q. Zhang, M. Li, Y. Song, J. Fan, C.-K. Wang, L. Lin, Theoretical study on the light-emitting mechanism of multifunctional thermally activated delayed fluorescence molecules, *J. Phys. Chem. C* 126 (2022) 2437–2446.
- [35] Y. Chen, S. Wang, X. Wu, Y. Xu, H. Li, Y. Liu, H. Tong, L. Wang, Triazatruxene-based small molecules with thermally activated delayed fluorescence, aggregation-induced emission and mechanochromic luminescence properties for solution-processable nondoped OLEDs, *J. Mater. Chem. C* 6 (2018) 12503–12508.
- [36] S. Xu, T. Liu, Y. Mu, Y.F. Wang, Z. Chi, C.C. Lo, S. Liu, Y. Zhang, A. Lien, J. Xu, An organic molecules with asymmetric structure exhibiting aggregation-induced emission, delayed fluorescence, and mechanoluminescence, *Angew. Chem. Int. Ed.* 54 (2015) 874–878.
- [37] M. Okazaki, Y. Takeda, P. Data, P. Pander, H. Higginbotham, A.P. Monkman, S. Minakata, Thermally activated delayed fluorescent phenothiazine-dibenzo[a,j]phenazine–phenothiazine triads exhibiting tricolor-changing mechanochromic luminescence, *Chem. Sci.* 8 (2017) 2677–2686.
- [38] B. Huang, Z. Li, H. Yang, D. Hu, W. Wu, Y. Feng, W. Jiang, B. Lin, Y. Sun, Bicolour electroluminescence of 2-(carbazol-9-yl)anthraquinone based on a solution process, *J. Mater. Chem. C* 5 (2017) 12031–12034.
- [39] B. Huang, W.-C. Chen, Z. Li, J. Zhang, W. Zhao, Y. Feng, B.Z. Tang, C.-S. Lee, Manipulation of molecular aggregation states to realize polymorphism, AIE, MCL, and TADF in a single molecule, *Angew. Chem. Int. Ed.* 57 (2018) 12473–12477.
- [40] K. Zheng, F. Ni, Z. Chen, C. Zhong, C. Yang, Polymorph-dependent thermally activated delayed fluorescence emitters: understanding TADF from a perspective of aggregation state, *Angew. Chem. Int. Ed.* 59 (2020) 9972–9976.

- [41] B. Huang, D. Jiang, Y. Feng, W.-C. Chen, Y. Zhang, C. Cao, D. Shen, Y. Ji, C. Wang, C.-S. Lee, Mechanochromic luminescence and color-tunable light-emitting devices of triphenylamine functionalized benzo[*d,e*]benzo[4,5]imidazo[2,1-*a*]isoquinolin-7-one, *J. Mater. Chem. C* 7 (2019) 9808–9812.
- [42] B. Huang, X. Gu, Y. Feng, Y. Zhang, D. Jiang, W.-C. Chen, G. Dai, Y. Ji, Q. Zhao, C.-S. Lee, Solid-state fluorophore based on π -extended heteroaromatic acceptor: polymorphism, mechanochromic luminescence, and electroluminescence, *Cryst. Growth Des.* 20 (2020) 2454–2461.
- [43] CCDC 2034919 (OC) and 2034918 (RC) contain the supplementary crystallographic data for this paper. These data can be obtained free of charge from The Cambridge Crystallographic Data Centre via, www.ccdc.cam.ac.uk/data_request/cif.
- [44] M.J. Frisch, Gaussian 09, Revision A.01, Gaussian, Inc., Wallingford, CT, 2009.
- [45] S.Y. Lee, T. Yasuda, Y.S. Yang, Q. Zhang, C. Adachi, Luminous butterflies: efficient exciton harvesting by benzophenone derivatives for full-color delayed fluorescence OLEDs, *Angew. Chem. Int. Ed.* 53 (2014) 6402–6406.
- [46] D. Liu, J.Y. Wei, W.W. Tian, W. Jiang, Y.M. Sun, Z. Zhao, B.Z. Tang, Endowing TADF luminophors with AIE properties through adjusting flexible dendrons for highly efficient solution-processed nondoped OLEDs, *Chem. Sci.* 11 (2020) 7194–7203.
- [47] S. Hirata1, Y. Sakai, K. Masui, H. Tanaka, S.Y. Lee, H. Nomura1, N. Nakamura, M. Yasumatsu, H. Nakanotani, Q. Zhang, K. Shizu, H. Miyazaki, C. Adachi, Highly efficient blue electroluminescence based on thermally activated delayed fluorescence, *Nat. Mater.* 14 (2015) 330–336.
- [48] Y. Ge, B. Huang, Light-emitting analogues based on triphenylamine modified quinoxaline and pyridine[2,3-*b*]pyrazine exhibiting different mechanochromic luminescence, *New J. Chem.* 45 (2021) 11304–11312.